Nanoscale

PAPER

View Article Online
View Journal | View Issue

Cite this: *Nanoscale*, 2024, **16**, 21794

Enhancing the efficiency of PVDF-based piezoelectric catalysis through water-induced polarization and a micro-nano-composite strategy†

Haitao Li,*[a] Yingying Zhang,[a,b] Han Dai,[a] Veronica Pereir,[c] Junfeng Zhao*[a] and Hiang Kwee Lee *[c,d]

Polyvinylidene fluoride (PVDF)-based piezoelectric catalysts show promise in mechanical force-driven catalysis due to their good biocompatibility, flexibility, and ease of fabrication. However, the catalytic activity of pristine PVDF is limited due to its low piezoelectric phase content (<20%), poor orientation, and low surface carrier concentration. Here, we introduce an efficient PVDF-based composite nano-catalyst (rGO/PVDF) with high piezoelectric catalytic performance. We achieve this by employing a composite strategy that combines nanoscale water-induced polarization with polar functional group-modified graphene (rGO) serving as a nanoelectrode. The nanoscale water polarization effect, together with the two-dimensional planar structure of PVDF and the modified graphene's polar functional groups, effectively induces orientation in the PVDF piezoelectric phase to increase the functional β phase content. As a result, the β phase content and crystallinity of rGO/PVDF reach 95% and 40%, respectively, which are 600% and 170% higher compared to those of pristine PVDF. This enhancement plays a crucial role in endowing the material with strong force-to-electricity conversion characteristics. Additionally, the surface-modified rGO also boosts PVDF's surface carrier concentration and provides active sites for catalysis on the rGO/PVDF composite. Notably, under optimized conditions, our catalyst achieves a ~99.1% degradation rate of organic pollutants (10 mg L^{-1}) after 12 minutes of sonication at 240 W and maintains a high efficiency of ~93.7% even at a 10 times higher pollutant concentration (100 mg L^{-1}). Our piezoelectric catalyst also demonstrates efficient H_2O_2 production at 95.8 mmol g_{rGO}^{-1} h^{-1}, which is ~9-fold and ~134-fold higher than those of untreated PVDF and previously reported PVDF-based piezoelectric catalysts, respectively. This work paves the way for the development of highly efficient PVDF-based piezoelectric catalysts, thereby offering valuable insights for the advancement of mechanically driven catalysis in the environmental, energy, and chemical sectors.

Received 6th August 2024,
Accepted 17th October 2024

DOI: 10.1039/d4nr03221g

rsc.li/nanoscale

1. Introduction

Piezoelectric catalysis offers a promising way to use mechanical force for driving molecular transformations, addressing environmental challenges and advancing greener industries.[1] When subjected to environmental mechanical stress, piezoelectric materials produce a piezoelectric field due to lattice deformation. This field triggers energy band bending or surface charge transfer in the material, facilitating redox reactions.[2] The effectiveness of piezoelectric catalysis largely relies on the careful selection and strategic design of the material. Among various material candidates, the polyvinylidene fluoride (PVDF)-based piezoelectric polymer stands out for its excellent biocompatibility, ease of casting, flexibility, and chemical stability.[3] However, conventional non-polarized PVDF materials show weak piezoelectric activity and are electrically insulating.[4,5] These limitations hinder efficient piezoelectric catalysis and their practical applications.

Traditional methods to modify PVDF, such as stretching, electric field polarization, electrospinning, and incorporating filler composites, have been demonstrated to improve piezoelectric catalysis performance.[6–9] However, these approaches

[a]*Laboratory of Advanced Light Alloy Materials and Devices, Postdoctoral Workstation of Nanshan Group Co., Ltd., Yantai Nanshan University, Longkou 265713, China. E-mail: htli@yzu.edu.cn, zhaojunfengcc@163.com*
[b]*School of Chemistry and Chemical Engineering, Yangzhou University, Yangzhou, 225002, PR China*
[c]*Division of Chemistry and Biological Chemistry, School of Chemistry, Chemical Engineering and Biotechnology, Nanyang Technological University, 21 Nanyang Link, 637371 Singapore. E-mail: hiangkwee@ntu.edu.sg*
[d]*Institute of Materials Research and Engineering, The Agency for Science, Technology and Research (A*STAR), 2 Fusionopolis Way, #08-03, Innovis 138634, Singapore*
†Electronic supplementary information (ESI) available. See DOI: https://doi.org/10.1039/d4nr03221g

often demand high energy consumption and specialized equipment, which contradict the principles of green and cost-effective preparation. To overcome this, the generation of self-polarized PVDF through the phase transformation technique has emerged as a green and energy-efficient solution. Common methods involve blending and casting to enhance self-polarized piezoelectric phase transformation/separation. Despite these efforts, the resulting piezoelectric phase content of PVDF-based composites seldom exceeds 62%, resulting in inadequate piezoelectric efficiency.[10,11] More recently, we have reported on a highly self-polarized PVDF catalytic material loaded with carbon nanotubes (CNTs) with a high piezoelectric phase content of 91% arising from the nanoscale polarization effect of water.[12] The inclusion of CNTs also increases carrier concentration at the material interface, enhancing piezoelectric catalytic activity. Nonetheless, the limited orientation of the piezoelectric phase and a scarcity of active sites on the piezoelectric material still restrict its overall catalytic performance.

Here, we propose using reduced graphene oxide (rGO) or graphene as co-catalytic materials to address existing challenges by capitalizing on their unique structural and chemical features, such as flexible structure, large specific surface area, high carrier mobility, and efficient electron conduction, for promoting energy collection and conversion processes.[13] More importantly, rGO-based materials can be easily modified with heteroatoms (such as N atoms) to increase their affinity with common reaction media like water and polar solvents.[13] The polar functional groups on their surfaces are crucial for enhancing wettability and facilitating ion migration at active sites, potentially improving both the electrochemical and catalytic performances of piezoelectric catalysts.

In this study, we achieve efficient piezoelectric catalysis by introducing multifunctional rGO/PVDF nanocomposites. Using PVDF as the base material, we realize a self-polarized PVDF with a high β-phase content *via* the nanoscale induction effect induced by water. We modify graphene with polar functional groups to serve as a nanoelectrode, providing the main active site as well as acting as a charge donor and piezoelectric enhancer for PVDF. Notably, our unique approach leads to self-polarized rGO/PVDF with a ~94% β phase content and ~40% crystallinity, surpassing those of the original PVDF by ~6-fold and ~2-fold, respectively. As proof-of-concept demonstrations, we apply the rGO/PVDF composite (1) to treat organic polluted wastewater and (2) catalytically produce H_2O_2. Using ultrasound-based mechanical energy (240 W), the rGO/PVDF nanocomposite effectively removes organic pollutants at high concentration (100 mg L^{-1}), reaching up to 94% degradation efficiency in just 2 hours. This unique piezoelectric catalyst also achieves a high H_2O_2 yield rate of 95.8 mmol g_{rGO}^{-1} h^{-1}, notably outperforming untreated PVDF (*i.e.* without rGO) and existing PVDF-based piezoelectric catalysts by ~9-fold and >130-fold, respectively. A mechanistic study reveals the critical roles of $^{\bullet}OH$ and $^{\bullet}O_2^-$ radicals as active species in the piezoelectric catalysis process. This work offers valuable insights into improving the piezoelectric catalytic properties of PVDF-based composites, with the aim of facilitating efficient mechanochemical molecular transformations for practical environmental, energy, and chemical applications.

Hiang Kwee Lee

Hiang Kwee Lee is a Nanyang Assistant Professor at the School of Chemistry, Chemical Engineering and Biotechnology at Nanyang Technological University. He earned both his Ph.D. and bachelor's degrees in Chemistry from Nanyang Technological University in 2018 and 2013, respectively. His research program combines chemistry, nanotechnology, materials sciences, and in operando *spectroscopy to develop next-generation catalytic ensembles aimed at addressing global energy and environmental crises.*

2. Experimental section

2.1 Materials

Polyvinylidene fluoride (PVDF, MW = 500 000), *N*,*N*-dimethylformamide (DMF, 99.5% purity), graphene oxide (GO), ethylene imine polymer (PEI) and potassium iodide (KI) were purchased from Shanghai Aladdin Biochemical Technology Co., Ltd. Rhodamine B (RhB), ammonium molybdate tetrahydrate ($H_{32}Mo_7N_6O_{28}$), and isopropyl alcohol (IPA) were obtained from Macklin, China. Ethylenediaminetetraacetic acid disodium salt dihydrate (EDTA-2Na) was obtained from Sigma-Aldrich, China. Hydrogen peroxide (H_2O_2), *p*-benzoquinone (BQ), and silver nitrate ($AgNO_3$) were purchased from Sinopharm Chemical Reagent Co., Ltd. All reagents were used without further purification.

2.2 Preparation of reduced graphene oxide (rGO)

0.15 g of graphene oxide (GO) was weighed into a 250 mL round bottom flask containing 50 mL of deionized water and subsequently sonicated for 5 min to homogenize the particle suspension. In addition, 0.3 g of potassium hydroxide and 3 g of ethylene imine polymer (PEI) were added into a beaker. 50 mL of deionized water was then added into the beaker and mixed well. The suspension in the beaker was subsequently added into the round bottom flask containing the GO suspension. The mixture was placed in an oil bath at 80 °C for 10 h. After reaction, the solution was centrifuged and washed with an ample amount of deionized water. The as-obtained rGO product was freeze-dried and stored for subsequent use.

2.3 Fabrication of the self-polarized rGO/PVDF nanocomposite

0.5 g of polyvinylidene fluoride (PVDF) powder was added to 50 mL of DMF, and a low concentration polyvinylidene fluor-

ide (PVDF) solution was prepared by stirring at 900 rpm and 25 °C for 2 h. Different mass fractions of rGO (w.r.t. PVDF, 0 wt%, 0.50 wt%, 1.00 wt%, 1.50 wt% and 2.00 wt%) were added to the solution mixture, and precursor solutions of self-polarized rGO/PVDF (SP/rGO$_x$, where x = 0, 0.5, 1.0, 1.5, and 2.0; SP denotes self-polarized PVDF in the nanocomposite) nanocomposites were obtained by continuous stirring until uniform dispersion. Subsequently, the precursor solutions were quickly poured into 2000 mL of deionized water to form SP/rGO$_x$ under the action of nanoscale water molecules. The solutions were then filtered and dried at room temperature to obtain self-polarized SP/rGO$_x$ nanocomposites that can be further used.

2.4 Piezoelectric catalysis activity measurements

2.4.1 Piezoelectric catalysis degradation of dye pollutants. The piezoelectric catalytic activity of the samples was evaluated based on the degradation of organic pollutants by ultrasonic treatment (an ultrasonic power of 240 W). Self-polarized rGO/PVDF (SP/rGO$_x$, 0.015 g) was added to a 20 mL vial containing pollutant aqueous solution (15 mL, 100 mg L^{-1}) and placed for 30 min in the dark to achieve adsorption/desorption equilibrium. By frequently changing the water in the ultrasonic cleaner, the temperature of the degradation reaction was controlled at 20 ± 2 °C. 1.5 mL of reaction solution was extracted at a pre-determined interval of 30 min for subsequent measurement using UV-visible absorption spectroscopy. The characteristic absorption wavelength of the contaminant solution at 553 nm was used to monitor changes in solution concentration. The degradation efficiency (%) was calculated using eqn (1):

$$\text{Dye degradation}\,(\%) = \frac{C_0 - C_t}{C_0} \times 100\% \quad (1)$$

where C_0 is the initial concentration of the pollutant solution and C_t is the concentration of the pollutant solution at reaction time t.

Moreover, scavenger experiments were also carried out to determine the active species generated during piezoelectric catalysis for mechanistic investigation. $AgNO_3$, EDTA-2Na, IPA, and BQ (1 mM) were used as trapping agents to verify the contributions of electrons (e^-), holes (h^+), hydroxyl radicals ($^{\bullet}OH$) and superoxide radicals ($^{\bullet}O_2^-$), respectively, in the piezoelectric catalytic degradation process.[14] SP/rGO$_x$ materials were collected after each piezoelectric catalytic reaction cycle, washed with a copious amount of ethanol and deionized water to remove residual pollutants, and dried in a vacuum at 60 °C for 24 h for subsequent tests.

2.4.2 Piezoelectric catalysis production of H_2O_2. The piezoelectric catalysts were also evaluated for H_2O_2 production driven by ultrasound (40 kHz, 300 W) under ambient air conditions. In a typical experimental setup, self-polarized rGO/PVDF (SP/rGO$_x$; 0.005 g) was dispersed in ethanol solution (10 mL, v/v: 1/4).[11] In addition, control experiments were carried out under high-purity O_2, Ar and N_2 atmospheres. The generated H_2O_2 content was determined by a colorimetric method.[15,16] Briefly, 500 μL of reaction solution was added to 2 mL of potassium iodide (KI, 0.1 M) and 50 μL of ammonium molybdate tetrahydrate ($H_{32}Mo_7N_6O_{28}$, 0.01 M) for 15 min. The reaction solution was collected and subsequently measured using a UV-visible absorption spectrometer. The characteristic peak intensity at 350 nm was used to monitor changes in H_2O_2 concentration. All the above reactions were carried out in the dark and under a controlled temperature environment of about 20 °C.

2.5 Instruments and characterization

A field emission scanning electron microscope (FESEM, S-4800, Hitachi Co., Japan) was used. XRD analysis was performed using a Rigaku D/Max-2500 X-ray diffractometer (Japan) with Cu Kα radiation (I = 1.5406 μm) operated at 40 kV and 200 mA. The samples were analyzed by Fourier transform infrared spectroscopy (FTIR) on an Antaris II. X-ray photoelectron spectroscopy (XPS) analysis of samples was performed using an ESCALAB 250 Xi (Thermo Scientific, America). A Bruker EMX 10/12 electron paramagnetic resonance (EPR, Bruker, Germany) spectrometer was used to detect the reaction products of the composites. The decomposition rate of dyes in solution was measured using a UV-6100 dual beam spectrophotometer (Mapada, China).

3. Results and discussion

3.1 Preparation and characterization of self-polarized rGO/PVDF nanocomposites

Fig. 1 illustrates the preparation process of self-polarized rGO/PVDF nanocomposites and their application as piezoelectric catalysts for organic pollutant degradation and H_2O_2 production. In brief, the precursor solution of rGO/PVDF was first prepared by dissolving PVDF powder in *N*,*N*-dimethylformamide (DMF), and nitrogen-doped rGO was then added as a conductive filler. Then rGO/PVDF was prepared by rapidly pouring the precursor solution into deionized water to form PVDF molecules by phase separation and precipitation. It is worth noting that the difference in the solubility of PVDF in DMF and water enables water molecules to induce polarity at the nanoscale, leading to the formation of self-polarized rGO/PVDF nanocomposites with a cross plane zigzag conformation of the β phase.[17] That is, the water induced method promotes the extensive interaction between water molecules and low concentration PVDF solution during the phase separation process, which promotes the effective self-polarization of PVDF. Moreover, the addition of rGO with polar functional groups shows good affinity for polar solvents, a crucial factor for enhancing its chemical interaction with target reactant molecules and facilitating ion migration on rGO/PVDF composites.[13,18,19] Under ultrasonication, the rGO/PVDF composite (Fig. 1) comprising nanoscopic rGO and microscopic self-polarized PVDF is anticipated to possess strong piezoelectric properties. Achieving efficient piezoelectric conversion is

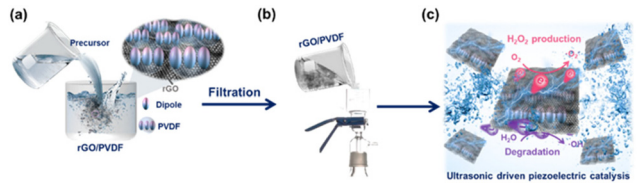

Fig. 1 Schematic diagram of the preparation process of the self-polarized rGO/PVDF nanocomposite and its application in piezoelectric catalysis. (a and b) Preparation process of rGO/PVDF composites. (c) Application of rGO/PVDF in piezoelectric catalytic degradation of organic pollutants and H_2O_2 production.

important for facilitating the separation of electron–hole pairs for enhanced piezoelectric catalysis (Fig. 1c).

3.2 Characterization of GO and rGO

To improve and understand the charge supply mechanism of rGO during piezoelectric catalysis, we modify the graphene oxide (GO) starting material with macromolecular ethylene imine polymer (PEI) in an alkaline potassium hydroxide environment. We subsequently analyze the surface morphology and structure of as-obtained rGO to unravel potential insights into the charge supply mechanism of rGO for the piezoelectric catalysis. As shown in Fig. 2(a), the color of GO changes from brown (left) to black (right) as it transforms into rGO after the modification process. Morphological characterization of rGO (Fig. S2†) reveals a smooth surface with sparse filamentous attachments and some randomly oriented folds.

Further UV-visible absorption analysis reveals significant changes before and after the modification of GO with PEI (Fig. 2a). Specifically, the disappearance of the absorption peak of GO at 230 nm, denoting its π–π* transition of aromatic C=C, indicates a successful reaction with PEI.[13] In addition, Fourier-transform infrared spectroscopy (FTIR) comparisons highlight clear differences in molecular bonding before and after GO modification (Fig. 2b). Initially, GO exhibits peaks corresponding to O–H bond stretching at 3210 cm^{-1}, C=C bond stretching at 1615 cm^{-1}, C=O bond stretching at 1723 cm^{-1}, and C–O bond stretching at 1168 cm^{-1} and 1049 cm^{-1}. PEI features in-plane N–H bond bending vibrations at 1592 cm^{-1} and 1461 cm^{-1}, and a C–N bond stretching vibration at 1293 cm^{-1}. After the modification, the FTIR spectrum of rGO retains the in-plane bending vibration of the N–H bond at 1646 cm^{-1} and 1550 cm^{-1}, and introduces a C–N bond stretching vibration peak at 1343 cm^{-1}. Notably, the epoxy C–O bond stretching peaks (*i.e.* 1168 cm^{-1} and 1049 cm^{-1}) initially present in GO disappear, denoting the successful reaction between GO and PEI to form rGO.[20–22]

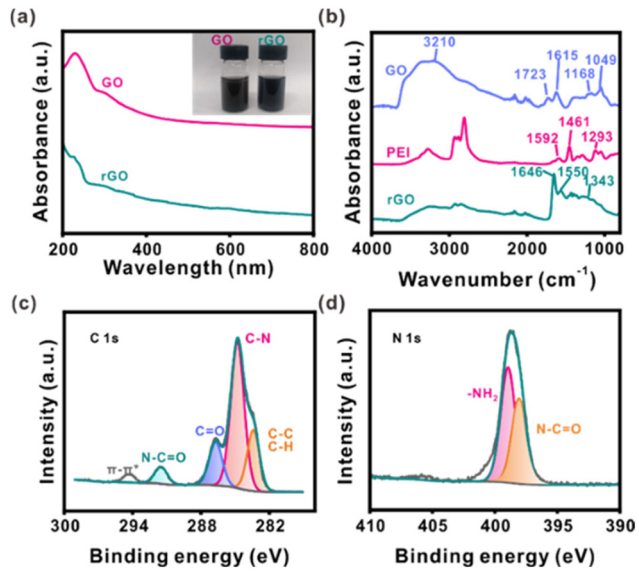

Fig. 2 Characterization of GO and rGO. (a) UV-visible absorption spectra of rGO before and after modification. Inset: corresponding optical image of the samples. (b) Fourier-transform infrared spectra of GO, PEI, and rGO. XPS spectral analysis of rGO: (c) C 1s spectrum and (d) N 1s spectrum.

We subsequently utilize X-ray photoelectron spectroscopy (XPS) to analyze the surface composition and chemical state of rGO (Fig. 2c and d).[23] The high-resolution C 1s XPS spectrum of rGO (Fig. 2e) reveals five distinct peaks with binding energies at 283.4 eV, 284.8 eV, 286.7 eV, 291.5 eV, and 294.3 eV, corresponding to the aliphatic carbon chain (C–C), amine group (C–N), carbonyl group (C=O), amide carbon (N–C=O), and amide group, respectively. Furthermore, the N 1s XPS spectrum of rGO (Fig. 2f) showcases two peaks at 398.1 eV and 399.1 eV that are indexed to $–NH_2$ and –N–C=O functional groups, respectively. This observation confirms the presence of amide bonds within rGO's chemical structure, a result of the ring-opening reaction between the epoxy groups in GO and amino groups in PEI. The incorporation of polar functional groups, such as amine group, carbonyl group, and amide bond, is crucial for enhancing rGO affinity with polar solvents.[13,18,19] These chemical interactions play a vital role in enhancing rGO interactions with target reactant molecules and improving the ion migration in PVDF composites. Both enhanced properties are anticipated to improve the electrochemical performance of the materials and their associated piezoelectric catalytic activity.

3.3 Characterization of rGO/PVDF nanocomposites

To elucidate the structural characteristics of self-polarized PVDF (SP) and its rGO/PVDF (SP/rGO) nanocomposites, we employ scanning electron microscopy (SEM) for detailed analysis. The SP/rGO nanocomposite is prepared by adding rGO with excellent conductivity into the PVDF matrix using a straightforward water-induced polarization method. SEM imaging reveals that the surface of the modified graphene oxide is slightly smooth, featuring some filamentous structures and partially random folds that closely resemble the rGO's original structure (Fig. 2b). The rGO is also observed to be deposited on the surface of spherical self-polarized PVDF (SP; *i.e.*, 0 wt% rGO) that has an average diameter of (175 ± 30) nm (Fig. 3c and Fig. S2a†). This morphology is attributed to the low concentration of PVDF used in the phase separation

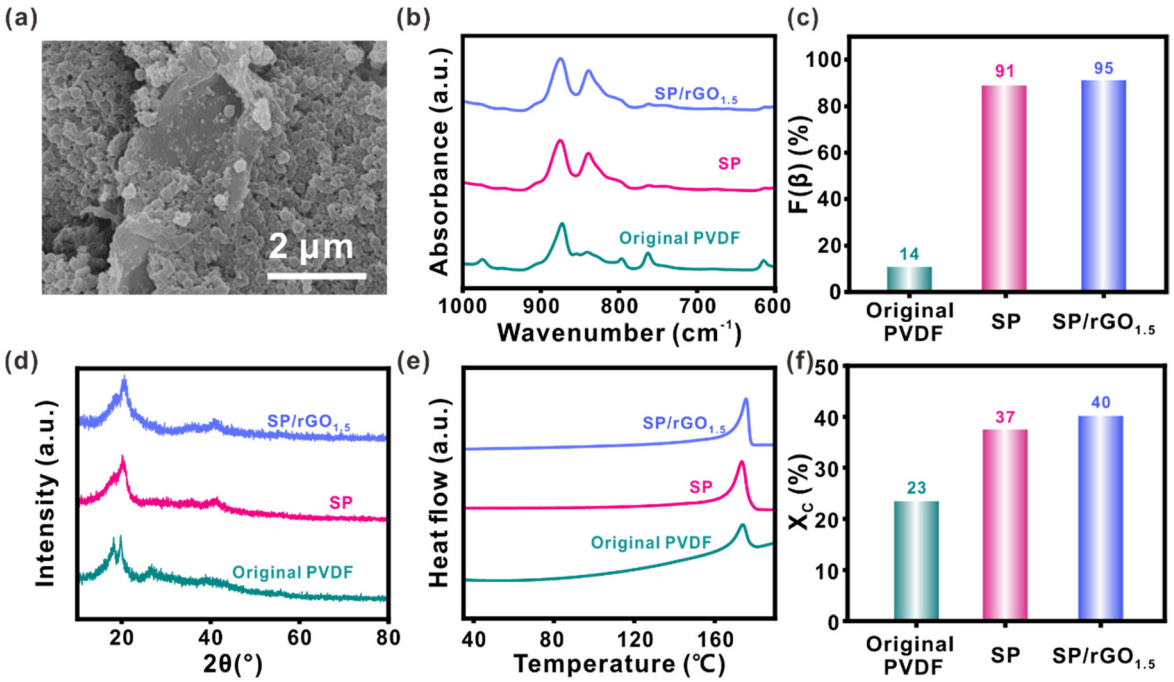

Fig. 3 Characterization of self-polarized rGO/PVDF composites. (a) SEM image of the rGO/PVDF composite. (b) FTIR spectra of the PVDF starting material, self-polarized PVDF (SP), and self-polarized rGO/PVDF nanocomposites (SP/rGO$_x$). (c) Corresponding calculated β phase content. (d) XRD pattern, (e) DSC heating curve, and (f) corresponding calculated crystallinity of various platforms.

process. When the conductive rGO flakes are added to the PVDF solution (SP/rGO$_{1.5}$, where 1.5 indicates that 1.5 wt% of rGO is added), the resulting nanocomposite exhibits a size similar to that of standalone SP (~180 ± 25 nm; Fig. S2b†). FTIR analysis of SP/rGO$_{1.5}$ confirms a significant increase in the piezoelectric phase β content to 91% (eqn (S1)†), which is ~6 times higher than that of the untreated PVDF material.[24] Interestingly, while the inclusion of rGO further enhances the β phase content of PVDF, the effect is smaller than the nanoscale water polarization effect. The formation of PVDF's β phase is primarily driven by the action of water molecules during the self-polarization process. The addition of rGO modestly improves PVDF's piezoelectric properties by fostering the electrostatic interaction between PVDF and rGO particles. This interaction promotes dipole deflection within PVDF, facilitating a transformation from the α phase to the more active β phase. The X-ray diffraction (XRD) patterns of both SP and SP/rGO$_{1.5}$ confirm an enhanced β phase composition in the nanocomposite compared to the original PVDF material (Fig. 3d).

In addition, the crystallinity of PVDF is another crucial factor for assessing its piezoelectric properties (*e.g.*, β phase order). Differential scanning calorimeter (DSC) characterization is utilized to determine the crystallinity of SP/rGO.[25] Fig. 3e shows the DSC heating curves of pristine PVDF powder, SP, and SP/rGO$_{1.5}$, revealing a shift towards higher crystallization temperatures. Specifically, the transition temperature increases from 160.0 °C for pristine PVDF to 161.81 °C for SP/rGO$_{1.5}$. The analysis determines that the crystallinity of SP/rGO$_{1.5}$ is ~40%, which represents an enhancement of ~2-fold over the original PVDF powder and 1.1-fold over self-polarized PVDF (Fig. 3f and eqn (S2)†). The elevated composition and crystallinity of the β phase in SP/rGO$_{1.5}$ are crucial for facilitating the subsequent conversion of mechanical energy into chemical energy. Moreover, integrating rGO as a conductive filler serves to improve charge carrier concentration (Fig. S3†) and the wettability of the composites (Fig. S4†). The results show that rGO modified with polar functional groups exhibits better wettability due to the presence of abundant heteroatoms.[13] These polar functional groups on the rGO surface demonstrate high affinity for aqueous solvents of similar polarity.[13,18,19] Such hydrophilic properties are beneficial for material wetting and ion migration, thereby promoting the chemical reactivity of the composite for enhanced piezoelectric catalysis.

3.4 Piezoelectric catalysis activity

3.4.1 Piezoelectric catalysis degradation. As a proof-of-concept application, we utilize SP/rGO as a piezoelectric catalyst for catalytic degradation of organic pollutants and production of H_2O_2. Rhodamine B (RhB) is selected as a model organic pollutant because it is a common water pollutant with serious toxicity and mutagenicity.[26] The reaction is performed by adding SP/rGO to the contaminant aqueous solution and placing it in the dark for 30 min to achieve adsorption/desorption equilibrium. Piezoelectric catalysis is subsequently initiated by subjecting the reaction setup to ultrasonication (240 W). The reaction is monitored by extracting an aliquot of the reaction solution at a predetermined interval of 30 min to quantify the pollutant concentration remaining in the reaction solution.

To optimize the piezoelectric catalyst, we first systematically investigate the effect of varying rGO compositions (0–2 wt%) on the catalytic performance. Our findings reveal that increasing the rGO content from 0 wt% to 1.5 wt% leads to a gradual increase in the degradation efficiency of RhB (initial concentration: 100 mg L^{-1}) from 45.0% to 93.7% (Fig. 4a), respectively. However, a further increase in the GO content beyond 1.5 wt% (*i.e.*, SP/$rGO_{2.0}$) results in a slight decrease in the degradation efficiency to 78.6%. Notably, the degradation efficiency of SP/$rGO_{1.5}$ is ~3.5-fold and ~27-fold higher than that of untreated PVDF and blank experiments (no catalyst; Fig. S5†), respectively, surpassing results reported in other studies (Table S1†).[27–29] The self-degradation of RhB in blank experiments primarily results from the cavitation effect under ultrasonic treatment.[30] It is worth noting that SP/$rGO_{1.5}$ exhibits high degradation ability for RhB at a concentration of 10 mg L^{-1}, achieving an efficiency of 99.1% within just 12 min. The initial increase in the degradation efficiency with more rGO loading is attributed to the enhanced surface carrier concentration by the rGO. The subsequent decline in the catalytic performance is due to an excessive increase in the composite's internal conductivity (*i.e.*, >1.5 wt% rGO loading), which promotes charge recombination. Compared to composites with various rGO mass loadings, SP/$rGO_{1.5}$ demonstrates the highest rate constant of 0.0243 min^{-1} (k; eqn (2) and Fig. 3b). Hence, we select SP/$rGO_{1.5}$ for further examination of its piezocatalytic performance and properties.[31]

$$\ln(C_0/C = kt) \quad (2)$$

We also evaluate the reusability of piezoelectric catalysts and their performance under different water conditions, focusing on (1) pH levels, (2) ambient temperatures, and (3) water qualities. SP/$rGO_{1.5}$ demonstrates high reusability, maintaining a degradation efficiency above 80% across three consecutive cycles (Fig. 4d). It also efficiently degrades high concentrations of RhB, with a degradation rate exceeding 85% across a broad pH range, from strongly acidic (pH 1) to weakly alkaline (pH 10). Notably, the efficiency only slightly decreases to ~78% even under strong alkaline conditions (pH 13), highlighting the compatibility of the SP/$rGO_{1.5}$ composite with diverse pH environments (Fig. S6†). Additionally, SP/$rGO_{1.5}$ maintains a degradation efficiency above 90% at ambient to slightly higher temperatures (20–40 °C), while the efficiency falls to around 77.3% at lower temperatures (10 °C; Fig. S7†). This result indicates the potential stability and effectiveness of SP/$rGO_{1.5}$ in degrading water pollutants in (sub)tropical regions. It is also noteworthy that SP/$rGO_{1.5}$ maintains its high catalytic performance in deionized water, tap water and sea water, with degradation efficiencies reaching 90% (Fig. S8†). SP/$rGO_{1.5}$ clearly stands out for its excellent recyclability, robust stability under various environmental conditions, and effective operation in different types of aqueous media.

To uncover the molecular mechanism driving the high degradation efficiency of SP/$rGO_{1.5}$, we use EDTA-2Na, $AgNO_3$, isopropyl alcohol (IPA), and benzoquinone (BQ) as trapping agents for holes (h^+), electrons (e^-), hydroxyl radicals ($^{\bullet}OH$), and superoxide radicals ($^{\bullet}O_2^-$), respectively. This comparison is vital for identifying the active agents and understanding

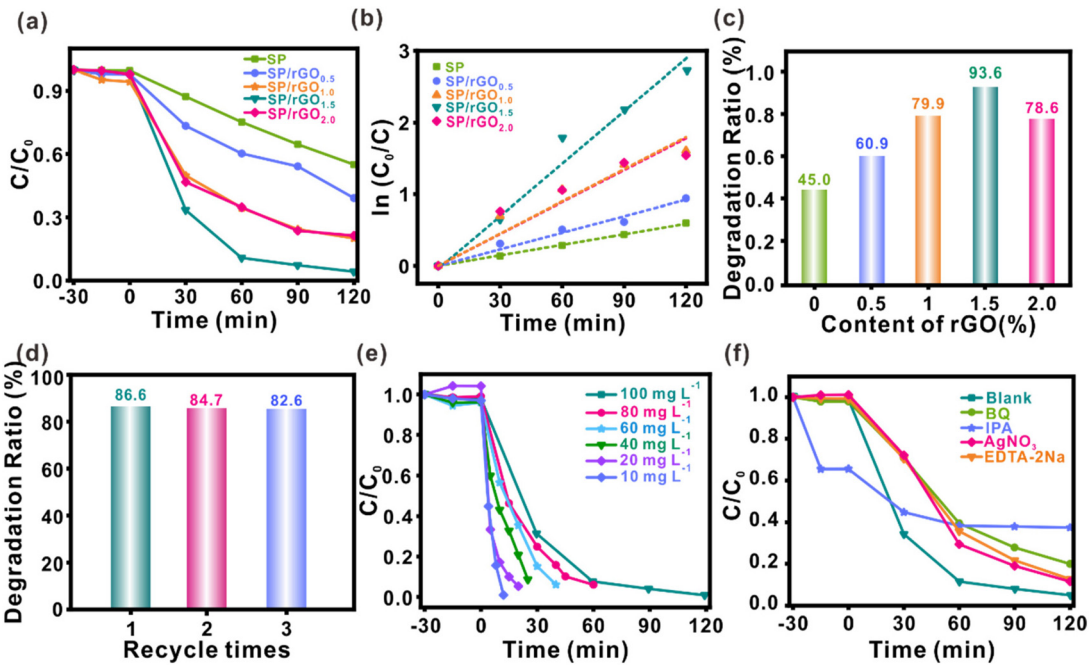

Fig. 4 Piezoelectric catalysis degradation of organic pollutants using SP/rGO. Time-dependent plot of (a) normalized RhB concentration (C/C_0) and (b) $\ln(C_0/C)$ using SP/rGO containing different rGO contents. Time-dependent plot of normalized concentration under (c) different ultrasonication powers and (d) the degradation ratios of RhB over three repeated cycles. Time-dependent plot of (e) normalized RhB concentration (C/C_0) at different initial concentrations and (f) when in the presence of different scavengers using SP/$rGO_{1.5}$ as the piezoelectric catalyst.

their roles in the degradation process.[32] The results show that both IPA and BQ have obvious inhibitory effects on the piezoelectric catalytic degradation process, which indicates that $^{\bullet}OH$ and $^{\bullet}O_2^-$ are the main active species produced by SP/rGO$_{1.5}$ during the ultrasonic process for the decomposition of organic pollutants. Electron paramagnetic resonance spectroscopy (ESR) further supports this observation (Fig. S9†), showing a marked increase in the peak intensities of $^{\bullet}OH$ and $^{\bullet}O_2^-$ from 0 to 15 minutes upon applying ultrasound. In contrast, there are no characteristic peaks of $^{\bullet}OH$ and $^{\bullet}O_2^-$ in the absence of ultrasonic treatment, highlighting that ultrasonication plays a vital role in generating $^{\bullet}OH$ and $^{\bullet}O_2^-$ active species necessary for degrading organic pollutants.

Having established the superior piezoelectric catalytic performance of SP/rGO, we further apply it for piezocatalytic H_2O_2 production and assess the associated catalytic efficiency at different rGO loadings (0–2.0 wt%; Fig. 5a) using a colorimetric method. In a typical reaction setup, we add SP/rGO to a water–ethanol solution (20% ethanol) and sonicate the reaction solution for 2 h using the optimized conditions of 300 W. At pre-defined time intervals, an aliquot of the reaction solution is extracted and the amount of H_2O_2 generated is quantified using a standard calibration curve based on the characteristic absorption peak at 350 nm.[14] Notably, we observe an increase in H_2O_2 production as the rGO content rises from 0 wt% to 1.5 wt% (Fig. 5a and b). However, increasing the rGO beyond 1.5 wt% to 2.0 wt% (SP/rGO$_{2.0}$) does not further enhance H_2O_2 production but instead slightly reduces it, highlighting that the 1.5 wt% rGO in the composite achieves the optimal H_2O_2 production. This finding aligns with our observations on the degradation of organic pollutants, re-affirming that a 1.5 wt% rGO content offers the best piezoelectric catalysis performance. Utilizing SP/rGO$_{1.5}$ as the optimized piezoelectric catalyst, we achieve a high H_2O_2 production rate of 95.8 mmol g_{rGO}^{-1} h^{-1}, which remains stable even over three reaction cycles (Fig. S10†). More importantly, the H_2O_2 production for SP/rGO$_{1.5}$ is ~9-fold and ~134-fold better than that of untreated PVDF and previous PVDF-based piezocatalytic designs (Fig. 5a and Table S1†), respectively. It is also worth mentioning that rGO alone is catalytically inactive, as evident from the negligible H_2O_2 production under the same sonication conditions (Fig. S11†). The slight production of H_2O_2 in the blank experiment is mainly driven by the cavitation effect under ultrasonic treatment.[30] Moreover, standalone SP (*i.e.*, no rGO) also yields a low H_2O_2 production of 209 μM after 2 hours.

Notably, the SP exhibits a poor piezoelectric catalytic performance despite possessing a high β phase content. This limitation is due to the low carrier density on the PVDF surface,[5] as demonstrated by comparing the electrochemical impedance spectra and piezoelectric current of SP and SP/rGO$_{1.5}$ (Fig. S3 and S12†). We note that SP/rGO$_{1.5}$ generates a higher piezoelectric current of 2.3 μA (ultrasonic power, 240 W; film size, 3 × 2 cm^2; and mass load, 1 mg cm^{-2}), ~3.8 times greater than that of SP. This improvement results from the lower impedance of SP/rGO$_{1.5}$, which enhances charge separ-

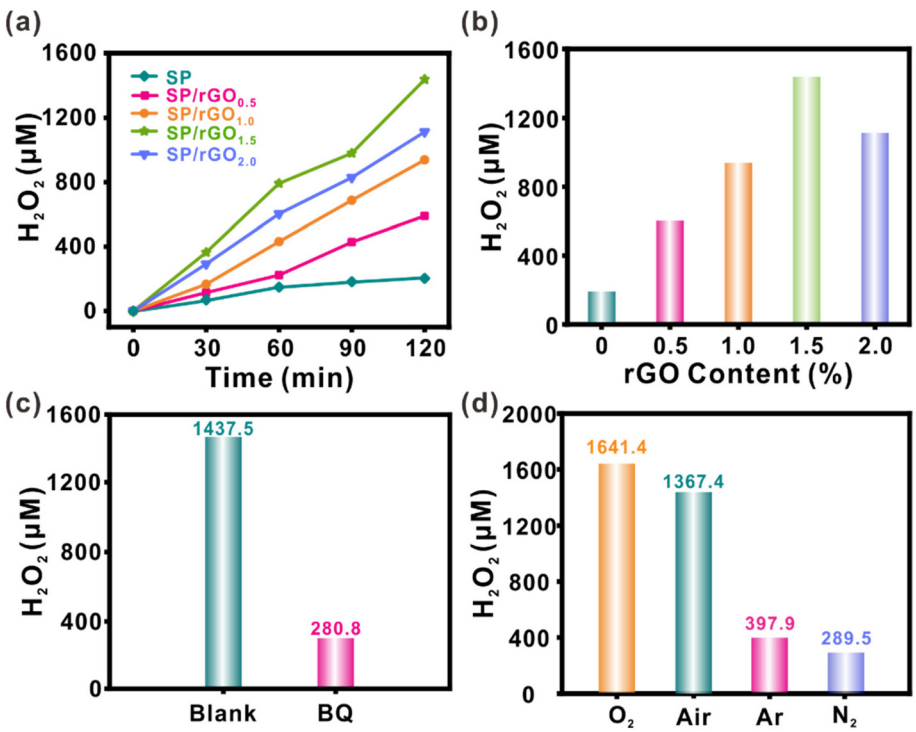

Fig. 5 Piezoelectric catalysis of SP/rGO to produce H_2O_2 under different conditions. (a) Effect of different rGO contents (0–2 wt%) in SP/rGO on piezocatalytic H_2O_2 production under 300 W ultrasound. (b) Comparison of H_2O_2 concentration produced by SP/rGO at different rGO loadings after 2 h. The concentration of H_2O_2 produced by SP/rGO (c) in the presence of a trapping agent and (d) under various gas environments after 2 h.

ation and transfer efficiency. The study thus underscores the effectiveness of the PVDF matrix with a high β phase content and the micro/nano-electrode (to be discussed later) composed of a conductive rGO filler doped with nitrogen in degrading organic pollutants and producing H_2O_2 with high piezoelectric activity.

To identify the active species for piezocatalytic H_2O_2, we perform additional control experiments using SP/$rGO_{1.5}$ as the piezoelectric catalyst and in the presence of benzoquinone (BQ) serving as an $^{\bullet}O_2^-$ capture agent.[33] In the presence of BQ, the amount of H_2O_2 produced by SP/$rGO_{1.5}$ within 2 h drops sharply from 1437.5 μM (*i.e.*, without BQ) to 280.8 μM (Fig. 5c). Electron paramagnetic resonance (ESR) confirms the generation of $^{\bullet}O_2^-$ species, with a clear increase in peak intensity from 0 to 15 minutes after ultrasound application. This observation indicates that $^{\bullet}O_2^-$ is the main active species to generate the H_2O_2 product *via* a two-step one-electron reduction process.[14] Moreover, we also study the H_2O_2 generation process using SP/$rGO_{1.5}$ under four different gas environments, namely (i) air, (ii) O_2, (iii) Ar, and (iv) N_2. Notably, the presence of an O_2 environment enables the highest H_2O_2 production of 1641.4 μM (Fig. 5d). Conversely, negligible H_2O_2 is produced under a control Ar or N_2 environment, highlighting that atmospheric oxygen is the primary source of the O_2 reactant rather than dissolved and/or trapped oxygen in the reaction solution. It should be noted that even under these conditions, a small amount of dissolved oxygen in the aqueous solution allows the piezoelectric H_2O_2 production to continue to a limited extent. Additionally, variations in oxygen content between water batches impact the reaction. Solutions under Ar usually contain more residual oxygen than those under N_2, resulting in slightly higher production, though the overall yield remains low. These systematic studies clearly demonstrate that the main chemical processes behind H_2O_2 generation involve the oxygen reduction reaction under an air or pure O_2 environment.

3.5 Mechanism discussion

Our findings underscore the significant role of sonication-induced charges in enhancing piezoelectric catalysis for both the degradation of organic pollutants and the production of H_2O_2 (Fig. 6). The polar functional groups on the modified graphene oxide's surface exhibit strong affinity towards solvents with similar polarity, improving wetting and ion migration within the material.[13,18,19] This enhancement in chemical properties facilitates better interaction with the aqueous reaction medium during piezoelectric catalysis. Sonication of SP/$rGO_{1.5}$ generates an internal electric field within the self-polarized PVDF, creating a micro/nano-electrode (SP/rGO) through the action of the polar functional group-modified conductive rGO filler. This piezoelectric field, under the micro/nano-electrode's influence, promotes the generation and separation of electron–hole pairs, driven by shock waves from the collapse of cavitation bubbles (Fig. 6). The enhanced charge separation consequently drives efficient redox reactions (eqn (2)). For the piezoelectric catalytic degradation of organic molecules, the pronounced

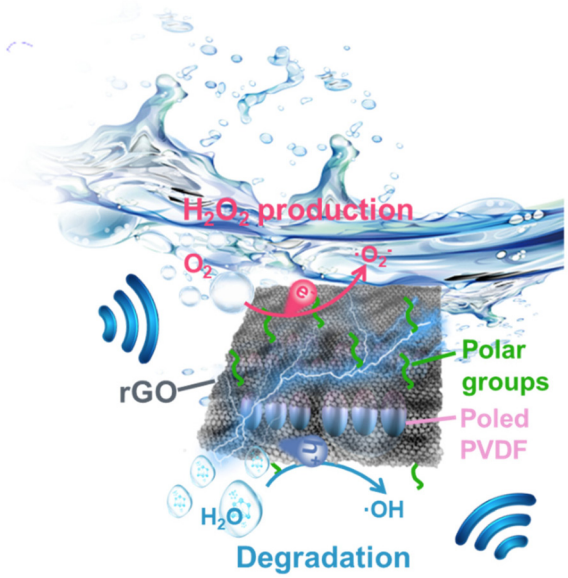

Fig. 6 Scheme illustrating the proposed mechanism of pollutant degradation and H_2O_2 production by piezoelectric catalysis.

degradation inhibition of RhB in the presence of IPA and BQ trapping agents highlights $^{\bullet}OH$ and $^{\bullet}O_2^-$ as the primary active species (eqn (3)–(9)). For the case of H_2O_2 generation, ethanol serves as a sacrificial agent to consume positive holes, allowing only the piezoelectrically generated negative electrons to contribute to H_2O_2 production. O_2 gas acts as the primary reactant in H_2O_2 generation, where polar oxygen molecules interact with the nitrogen atoms, which function as active sites on the rGO surface. These chemical interactions facilitate oxygen molecule adsorption on the rGO surface. Additionally, the polar functional groups' affinity with the aqueous solvent aids in wetting and ion migration, enhancing the material's electrochemical performance for better interaction with the aqueous medium during piezoelectric catalysis.[13] These phenomena consequently promote the transfer of mechanically driven piezoelectric electrons into oxygen species through the unique micro/nano-electrode design comprising rGO and self-polarized PVDF. Collectively, our study highlights the critical role of the internal piezoelectric field in enabling the effective separation of electrons and holes, which is an important attribute to promote mechanically driven redox reactions (eqn (3)–(9)).

$$SP/rGO_{1.5} + \text{ultrasound} \rightarrow e^- + h^- \quad (3)$$

$$H_2O \rightarrow OH^- + H^+ \quad (4)$$

$$e^- + O_2 \rightarrow {}^{\bullet}O_2^- \quad (5)$$

$$2H^+ + O_2 + 2e^- \rightarrow H_2O_2 \quad (6)$$

$$e^- + H_2O_2 + H^+ \rightarrow {}^{\bullet}OH + H_2O \quad (7)$$

$$OH^- + h^+ \rightarrow {}^{\bullet}OH \quad (8)$$

$$^{\bullet}OH/{}^{\bullet}O_2^- + \text{pollutants} \rightarrow \text{oxidation products} \quad (9)$$

4. Conclusion

In summary, we introduce a self-polarized rGO/PVDF composite as an efficient piezoelectric catalyst by exploiting a unique water-induced polarization approach and polar functional group-modified graphene as a nanoelectrode. Notably, the nano-induced effect of water molecules significantly enhances the β phase content and orientation. The addition of the polar functional group-modified rGO filler also improves the conductivity and ion migration of the composite material, thereby enabling an in-built nanoelectrode while providing the main active sites for piezoelectric catalysis. Together with the internal electric field of self-polarized PVDF, this approach boosts carrier density and optimizes the piezoelectric catalytic performance of the composite. This unprecedented strategy results in an increase in the β phase composition and crystallinity of SP/$rGO_{1.5}$ to 95% and 40%, respectively, which are 600% and 170% higher than those of the pristine PVDF material. Under 240 W sonication treatment, SP/$rGO_{1.5}$ demonstrates rapid and efficient catalytic degradation of pollutants, achieving 99.1% degradation efficiency for 10 mg L^{-1} RhB within 12 min and a ~94% efficiency for high-concentration RhB (100 mg L^{-1}) after 2 hours. Moreover, the nanocomposite also exhibits excellent reusability and adaptability to various environmental conditions, including pH, temperature, and water quality. Notably, the H_2O_2 production rate of SP/$rGO_{1.5}$ reached 95.8 mmol $g_{rGO}{}^{-1}$ h^{-1}, significantly outperforming the original PVDF and previous PVDF-based piezoelectric catalysts by approximately 9-fold and 134-fold, respectively. Mechanistic studies underline the critical role of the synergistic coupling between the PVDF matrix with a high β phase and the conductive, nitrogen-modified rGO filler in boosting the piezoelectric catalytic activity of SP/rGO for pollutant degradation and H_2O_2 production. The strategy of integrating rGO as a nanoelectrode offers a novel approach for designing PVDF-based composites to improve their piezoelectric properties and conductivity. Our work thus offers valuable insights for paving the way for the advancement of mechanically driven catalysis in environmental, energy, and (bio) chemical applications.

Data availability

The data supporting this article have been included as part of the ESI.†

Conflicts of interest

The authors declare no conflict of interest.

Acknowledgements

Haitao Li acknowledges the financial support from the Natural Science Foundation of Shandong Province (ZR2023QF019), H. K. L. acknowledges the funding support from the Singapore Ministry of Education (RS13/20 and RG4/21), Agency for Science, Technology and Research, Singapore (A*STAR, A2084c0158), Center of Hydrogen Innovation, National University of Singapore (CHI-P2022-05), and Nanyang Technological University start-up grants. Han Dai acknowledges the financial support from the Shandong Provincial Youth Innovation Science and Technology Project of Colleges and Universities (Grant No. 2021KJ089).

Notes and references

1 F. Bößl and I. Tudela, *Curr. Opin. Green Sustain. Chem.*, 2021, **32**, 100537.
2 M. C. Sekhar, E. Veena, N. S. Kumar, K. C. B. Naidu, A. Mallikarjuna and D. B. Basha, *Cryst. Res. Technol.*, 2022, **58**, 2200130.
3 T. D. Usher, K. R. Cousins, R. Zhang and S. Ducharme, *Polym. Int.*, 2018, **67**, 790–798.
4 X. Liu, Y. Shang, J. Zhang, C. Zhang and Interfaces, *ACS Appl. Mater. Interfaces*, 2021, **13**, 14334–14341.
5 B. Ponraj, R. Bhimireddi and K. B. R. Varma, *J. Adv. Ceram.*, 2016, **5**, 308–320.
6 E. S. Cozza, O. Monticelli, E. Marsano and P. Cebe, *Polym. Int.*, 2012, **62**, 41–48.
7 J.-Y. Ren, Q.-F. Ouyang, G.-Q. Ma, Y. Li, J. Lei, H.-D. Huang, L.-C. Jia, H. Lin, G.-J. Zhong and Z.-M. Li, *Macromolecules*, 2022, **55**, 2014–2027.
8 D. H. Kang and H. W. Kang, *Appl. Surf. Sci.*, 2016, **387**, 82–88.
9 R. Sahoo, S. Mishra, A. Ramadoss, S. Mohanty, S. Mahapatra and S. K. Nayak, *Mater. Res. Bull.*, 2020, **132**, 111005.
10 L. Wang, Z. Chen, Y. Zhang, C. Liu, J. Yuan, Y. Liu, W. Ge, S. Lin, Q. An and Z. Feng, *Chem.– Asian J.*, 2022, **17**, e202200278.
11 Z. Chen, J. Zhuang, C. Liu, M. Chai, S. Zhang, K. Teng, T. Cao, Y. Zhang, Y. Hu, L. Zhao and Q. An, *ChemElectroChem*, 2022, **9**, e202200124.
12 Y. Zhang, C. Chong, W. Tong, H. Li, H. K. Lee and J. Han, *Colloids Surf., A*, 2023, **677**, 132412.
13 M. Yang and Z. Zhou, *Adv. Sci.*, 2017, **4**, 1600408.
14 C. Wang, F. Chen, C. Hu, T. Ma, Y. Zhang and H. Huang, *Chem. Eng. J.*, 2022, **431**, 133930.
15 C. Karami and M. A. Taher, *J. Electroanal. Chem.*, 2019, **847**, 113219.
16 S. Lin, Q. Wang, H. Huang and Y. Zhang, *Small*, 2022, **18**, 2200914.
17 W. Tong, Q. An, Z. Wang, Y. Li, Q. Tong, H. Li, Y. Zhang and Y. Zhang, *Adv. Mater.*, 2020, **32**, 2003087.
18 G. F. Han, F. Li, W. Zou, M. Karamad, J. P. Jeon, S. W. Kim, S. J. Kim, Y. Bu, Z. Fu, Y. Lu, S. Siahrostami and J. B. Baek, *Nat. Commun.*, 2020, **11**, 2209.
19 N. Wang, L. Cheng, Y. Liao and Q. Xiang, *Small*, 2023, **19**, e2300109.

20 C. Liu, Y. Guo and D. Wang, *Tribol. Int.*, 2019, **140**, 105851.
21 H. Liu, C. Liu, S. Peng, B. Pan and C. Lu, *Carbohydr. Polym.*, 2018, **182**, 52–60.
22 M. Sharma, G. Madras and S. Bose, *Cryst. Growth Des.*, 2015, **15**, 3345–3355.
23 K. Roy, S. K. Ghosh, A. Sultana, S. Garain, M. Xie, C. R. Bowen, K. Henkel, D. Schmeiβer and D. Mandal, *ACS Appl. Nano Mater.*, 2019, **2**, 2013–2025.
24 S. Huang, S. Hong, Y. Su, Y. Jiang, S. Fukushima, T. M. Gill, N. E. D. Yilmaz, S. Tiwari, K.-i. Nomura, R. K. Kalia and Flame, *Combust. Flame*, 2020, **219**, 467–477.
25 C. Merlini, G. Barra, T. M. Araujo and A. Pegoretti, *RSC Adv.*, 2014, **4**, 15749–15758.
26 S. Varjani, P. Rakholiya, H. Y. Ng, S. You and J. A. Teixeira, *Bioresour. Technol.*, 2020, **314**, 123728.
27 X. Zhou, Q. Sun, Z. Xiao, H. Luo and D. Zhang, *J. Environ.*, 2022, **10**, 108399.
28 X. Cheng, Z. Liu, Q. Jing, P. Mao, K. Guo, J. Lu, B. Xie and H. Fan, *J. Colloid Interface Sci.*, 2023, **629**, 11–21.
29 L. Jiang, N. Xie, Y. Hou, H. Fu, J. Zhang, H. Gao and Y. Liao, *Catal. Commun.*, 2023, **181**, 106735.
30 C. Yi, Q. Lu, Y. Wang, Y. Wang and B. Yang, *Ultrason. Sonochem.*, 2018, **43**, 156–165.
31 X. Liao, X. Chen, Y. Tang, M. Zhu, H. Xie, Y. Xin, Y. Lin and X. Fan, *ACS Appl. Mater. Interfaces*, 2023, **15**, 1286–1295.
32 W. Ma, B. Yao, W. Zhang, Y. He, Y. Yu and J. Niu, *Chem. Eng. J.*, 2021, **415**, 129000.
33 H.-T. Vuong, D.-V. Nguyen, P. P. Ly, P. D. M. Phan, T. D. Nguyen, D. D. Tran, P. T. Mai and N. H. Hieu, *ACS Appl. Nano Mater.*, 2022, **6**, 664–676.